The Astrophysical Journal, 977:240 (11pp), 2024 December 20 https://doi.org/10.3847/1538-4357/ad946f

Turbulent Transport Characteristics of the Particles within Pulsar Wind Nebulae 3C58 and G54.1+0.3

Fang-Wu Lu[1,2], Bo-Tao Zhu[2,3], Wen Hu[2,4], and Li Zhang[2]
[1] Department of Physics, Yuxi Normal University, Yuxi, 653100, People's Republic of China
[2] Department of Astronomy, Key Laboratory of Astroparticle Physics of Yunnan Province, Yunnan University, Kunming 650091, People's Republic of China; lizhang@ynu.edu.cn
[3] College of Science, Yunnan Agricultural University, Kunming, 650201, People's Republic of China
[4] Department of Physics, Jinggangshan University, Ji'an, 343009, Jiangxi, People's Republic of China
Received 2024 April 16; revised 2024 November 7; accepted 2024 November 17; published 2024 December 18

Abstract

Turbulent transport characteristics of the particles within two Crab-like pulsar wind nebulae (PWNe), 3C58 and G54.1+0.3, are investigated in the framework of a time-dependent turbulent diffusion model. The model takes the gyroresonant interactions between the particles and turbulent waves into account, which enables us to self-consistently determine the energy and spatial coefficients of particles within the nebula via the distributions of turbulent waves. Our application of the model to the multiband emission from 3C58 and G54.1+0.3 reveals the following. (1) The energy and spatial diffusion coefficients seem to follow quasi-linear distributions in the Kolmogorov-type turbulence, but consistent with nonlinear distributions at low energies in the Kraichnan-type turbulence due to the effects of the turbulent scattering. (2) The stochastic acceleration and spatial diffusion processes may play a role in modifying the electron spectrum in the Kolmogorov-type turbulence, whereas in the Kraichnan-type turbulence the energy exchange between the turbulent waves and particles is more efficient, resulting in more significant effects of the stochastic acceleration and spatial diffusion processes on the electron spectrum at the low energies of $E_e \lesssim 1$ TeV. (3) At the high energies of $E_e \gtrsim 1$ TeV, the diffusion transport appears to be less effective for the evolution of the particles within 3C58 and G54.1+0.3 because the synchrotron radiative cooling process dominates over the particle transport. These two Crab-like PWNe are expected to be electron PeVatrons in the Galaxy, with a common slow diffusion escape occurring in both 3C58 and G54.1+0.3.

Unified Astronomy Thesaurus concepts: Pulsars (1306); Pulsar wind nebulae (2215); Supernova remnants (1667)

1. Introduction

Pulsar wind nebulae (PWNe) are one of the largest Galactic source classes at the TeV or even to the PeV γ-ray energies (H.E.S.S. Collaboration et al. 2018a; Z. Cao et al. 2024). It is generally believed that a PWN is formed when a relativistic magnetized wind interacts with the surrounding medium (e.g., P. Goldreich & W. H. Julian 1969; C. F. Kennel & F. V. Coroniti 1984a). The magnetized wind, composed of high-energy particles and magnetic fluxes, is powered by the associated pulsar releasing its rotational energy (e.g., C. F. Kennel & F. V. Coroniti 1984b). The majority of PWNe have been observed to emit photons with energies ranging from radio to TeV γ-rays. As a result, they provide essential information that enables us to understand fundamental physical processes occurring in PWNe, such as particle transport and acceleration.

The multiband nonthermal radiation in a PWN is typically thought to be produced by relativistic electrons via synchrotron and inverse Compton (IC) scattering processes (e.g., C. F. Kennel & F. V. Coroniti 1984b; O. C. de Jager & A. K. Harding 1992; A. M. Atoyan & F. A. Aharonian 1996; F. Aharonian et al. 2004; L. Zhang et al. 2008; J. Martin et al. 2012; F.-W. Lu et al. 2017; B.-T. Zhu et al. 2021), with the high-energy particles originating from the associated pulsar. Additionally, before being injected into the nebula, the particles released from the pulsar are believed to have accelerated extreme relativistic energy at the pulsar wind termination shock (TS; S. P. Reynolds & R. A. Chevalier 1984; A. M. Atoyan & F. A. Aharonian 1996). In this scenario, as the particles propagate away from the pulsar, they will unavoidably experience energy loss via adiabatic, synchrotron radiation, and IC scattering processes. Consequently, diffusion transport is expected to play a significant role in reducing the propagation time of the particles across the nebula, thereby mitigating the effects of radiative cooling processes on the particle spectrum (e.g., B. M. Gaensler & P. O. Slane 2006; M. J. Vorster & H. Moraal 2013; H. Abdalla et al. 2020; F.-W. Lu et al. 2020).

The diffusion coefficient of particles within PWNe is generally believed to be dependent on the structure of the magnetic field and the energy of the particles (e.g., I. Lerche & R. Schlickeiser 1981; R. A. Caballero-Lopez et al. 2004). However, the precise nature of diffusion transport in the nebula remains unclear. The observations of cosmic rays indicate that the particle diffusion in the Galaxy would follow an energy-dependent function with $D_{RR} = D_{RR,0}(E_e/1\ \mathrm{GeV})^{\delta}$, where $\delta = 0.3-0.6$ is the diffusion index, and $D_{RR,0} = (3-5) \times 10^{28}\ \mathrm{cm^2\ s^{-1}}$ is the diffusion coefficient at an electron energy of 1 GeV (A. W. Strong et al. 2007, and references therein). Furthermore, according to the magnetostatic quasi-linear theory, the relationship between the diffusion coefficient and magnetic field can be modeled as $D_{RR} \propto B^{-\delta}$ (e.g., I. Lerche & R. Schlickeiser 1981). These prescriptions have been extensively employed to investigate the diffusion transport mechanisms of the particles within PWNe (e.g., L. Zhang et al. 2008; X. Tang & R. A. Chevalier 2012; M. J. Vorster & H. Moraal 2013;

A. U. Abeysekara et al. 2017; R.-Y. Liu & H. Yan 2020; F.-W. Lu et al. 2023a; B.-T. Zhu et al. 2023).

It should be noticed that the diffusion transport of particles within PWNe would be affected by the turbulent magnetic fields, resulting in the turbulent scattering processes being instrumental in the energy-dependent diffusion transport (e.g., N. Bucciantini et al. 2011; O. Porth et al. 2014, 2016; J. Zrake & J. Arons 2017). In a turbulent environment, the particles will gain energy from the turbulent waves via gyroresonant interactions, which act as an energy diffusion and/or a stochastic acceleration of the particles within PWNe. In these processes, the turbulent energy will be consumed by the acceleration of particles, ultimately resulting in the release of particle confinement within the nebula and facilitating their diffusion and escape from the acceleration region (J. A. Miller & D. A. Roberts 1995; J. A. Miller et al. 1996). Therefore, the energy and spatial diffusion coefficients of the particles within a turbulent PWN would be mainly determined by the distribution of the turbulent waves (e.g., J. Skilling 1975; K. Fang et al. 2019).

Based on the above-mentioned considerations, and in combination with the views that the rapid diffusion is presumably oriented along the magnetic field and slower diffusion to the perpendicular direction within the nebula (e.g., O. Porth et al. 2016), a turbulent diffusion model was recently proposed by F.-W. Lu et al. (2023b) investigating the diffusion transport of the particles within turbulent PWNe. They applied the model to the prototype PWN, i.e., Crab Nebula, and found that the energy distribution of the diffusion coefficients can be determined self-consistently by the turbulent waves and the acceleration and spatial diffusion processes may play a role in modifying the electron spectrum.

In this paper, we use the turbulent diffusion model proposed by F.-W. Lu et al. (2023b) to investigate turbulent diffusion characteristics of particles within 3C58 and G54.1+0.3, with the aim of understanding particle diffusion transport within Crab-like PWNe. These two PWNe have been observed across radio, X-ray, and γ-ray bands and are commonly referred to as Crab-like PWNe because their morphologies and nonthermal spectra displayed in the X-ray band are similar to those found in the Crab Nebula (A. S. Wilson & K. W. Weiler 1976; W. Reich et al. 1985; T. Velusamy & R. H. Becker 1988; F. J. Lu et al. 2001; P. Slane et al. 2004). The organization of this paper is as follows. In Section 2, we give a brief description of the turbulent diffusion model. In Section 3, the applications of the model to the multiband emission from 3C58 and G54.1+0.3 are presented, and the turbulent transport characteristics of the particles are investigated. Finally, the discussion and conclusions are given in Section 4.

2. Model Description

In this section, we give a brief description of our turbulent diffusion model of PWNe (F.-W. Lu et al. 2023b). In the model, the energy injected from the associated pulsar into the PWN is considered to be split between the turbulent waves and electrons/positrons. Additionally, the particles are considered to have been accelerated to extreme relativistic energy at the TS before being injected into the nebula. In this scenario, the charged particles traveling across the nebula are expected to interact with the turbulent waves, serving as the damping effect for the turbulent waves and the energy and spatial diffusion processes for the particles within the nebula, respectively. Therefore, scattering and diffusion of the particles within PWNe could be strongly dependent on the characteristics of turbulent waves.

The properties of turbulent waves in PWNe would be extremely complex (e.g., O. Porth et al. 2014). However, X-ray observations imply that rapid diffusion is likely oriented along the magnetic field, while slow diffusion may occur in the perpendicular direction within PWNe (e.g., X. Tang & R. A. Chevalier 2012; O. Porth et al. 2016). Consequently, we only consider the gyroresonant interaction with the magneto-hydrodynamic (MHD) wave turbulence propagating parallel or antiparallel to the magnetic field in this paper. Additionally, MHD waves, serving as magnetic scattering centers in the stochastic acceleration scenario, mainly consist of three types: incompressible Alfvén modes, and compressible fast and slow modes (J. Cho & A. Lazarian 2002), and compressed MHD turbulence could more effectively scatter the particles (e.g., G. P. Zank & W. H. Matthaeus 1992; J. Cho & A. Lazarian 2003). Therefore, two classical types of compressible turbulence are taken into account in our model, i.e., Kolmogorov-type and Kraichnan-type turbulence (A. Kolmogorov 1941; R. H. Kraichnan 1965).

For a spin-down pulsar, the evolution of the luminosity is given by (e.g., F. Pacini & M. Salvati 1973)

$$L(t) = \frac{L_{\rm sd}}{(1 + T_{\rm age}/\tau_0)^{-\frac{n+1}{n-1}}}\left[1 + \frac{t}{\tau_0}\right]^{-\frac{n+1}{n-1}}, \quad (1)$$

where n is the braking index, $L_{\rm sd}$ is the current luminosity, $T_{\rm age}$ is the age of the pulsar, and $\tau_0 = 2\tau_{\rm c}/(n-1) - T_{\rm age}$ is the initial spin-down timescale, with $\tau_{\rm c}$ the characteristic age of the pulsar. According to B. M. Gaensler & P. O. Slane (2006), the age of the pulsar can be calculated with

$$T_{\rm age} = \begin{cases} 2\tau_{\rm c}\ln\left(\dfrac{P}{P_0}\right), & n = 1 \\ \dfrac{2\tau_{\rm c}}{n-1}\left[1 - \left(\dfrac{P_0}{P}\right)^{n-1}\right], & n \neq 1 \end{cases}, \quad (2)$$

where P_0 and P are the initial and current rotation period of the pulsar, respectively.

In our model, the evolution of the turbulent waves in the wavenumber space (k-space), which includes the turbulent cascade, damping, and adiabatic cooling processes, is described with

$$\frac{\partial W}{\partial t} = \frac{\partial}{\partial k}\left[k^2 D_{\rm kk}\frac{\partial}{\partial k}\left(\frac{W}{k^2}\right)\right] - \Gamma_{\rm k} W - \frac{\partial}{\partial k}[\dot{k}_{\rm ad} W] - \frac{W}{\tau_{\rm alf}} + Q_{\rm k,inj}(k, t), \quad (3)$$

where $W \equiv W(k, t)$ [erg · cm] is the distribution of the turbulent waves, k [cm^{-1}] is the wavenumber of the waves, $\Gamma_{\rm k}$ is the damping effect, $\dot{k}_{\rm ad}$ is adiabatic loss rate, $\tau_{\rm alf} = R(t)/\nu_{\rm A}(t)$ is the Alfvén sound crossing timescale with $R(t)$ and $\nu_{\rm A}(t)$ the radius of the nebula and Alfvén velocity of the waves, respectively, and $D_{\rm kk}$ is the diffusion coefficient of the turbulent waves which depends on the cascade phenomenology.

On the other hand, the evolution of the particles in the energy space (γ-space) can be described with the Fokker–

Planck equation, that is

$$\frac{\partial N}{\partial t} = \frac{\partial}{\partial \gamma}\left[\gamma^2 D_{\rm EE}\frac{\partial}{\partial \gamma}\left(\frac{N}{\gamma^2}\right)\right] - \frac{N}{\tau_{\rm diff}} - \frac{\partial}{\partial \gamma}[\dot{\gamma} N] + Q_{\rm e,inj}(\gamma, t), \quad (4)$$

where $N \equiv N(\gamma, t)$ is the distribution of the electrons, $D_{\rm EE}$ is the energy diffusion coefficient, $\tau_{\rm diff} = R^2(t)/D_{\rm RR}$ is the escape timescale due to spatial diffusion, with $D_{\rm RR}$ the spatial diffusion coefficient, and $\dot{\gamma}$ is the total energy loss rate of the electrons.

The function $Q_{\rm k,inj}(k, t)$ on the right-hand side of Equation (3) represents the injected turbulent waves, which is given by (e.g., J. A. Miller & D. A. Roberts 1995; J. A. Miller et al. 1996; K. Fang et al. 2019)

$$Q_{\rm k,inj}(k, t) = Q_{\rm w,0}(t)\delta(k - k_{\rm inj}), \quad (5)$$

denoting the waves are injected on a monoscale of $k_{\rm inj} = 2\pi/R(t)$, with $R(t)$ the radius of the nebula. Meanwhile, the normalization constant $Q_{\rm w,0}(t)$ for the injection spectrum can be calculated with $\eta_{\rm w} L(t) = \int_0^\infty Q_{\rm k,inj}(k, t)dk$, where $\eta_{\rm w}$ is the fraction of the pulsar spin-down luminosity converted into the turbulent energy.

In the Kolmogorov phenomenology, turbulent waves of comparable wavelengths are expected to interact with each other in about one eddy turnover time, which is then regarded as the timescale for spectral energy transfer to smaller wavelength fluctuations. On the other hand, in the Kraichnan treatment, the interaction timescale is assumed to be the Alfvén crossing time for a fluctuation, which is significantly shorter than that in the Kolmogorov case. Moreover, according to Y. Zhou & W. H. Matthaeus (1990) and J. A. Miller et al. (1996), the diffusion coefficient of these two phenomenologies can be written as

$$D_{\rm kk} = \begin{cases} k^3\beta_{\rm w}(t)c\left[\dfrac{kw(k, t)}{2u_{\rm B}(t)}\right]^{1/2} & \text{(Kolmogorov)} \\ k^3\beta_{\rm w}(t)c\left[\dfrac{kw(k, t)}{2u_{\rm B}(t)}\right] & \text{(Kraichnan)} \end{cases}, \quad (6)$$

where $\beta_{\rm w}(t) = \nu_{\rm A}(t)/c$ is the Alfvén velocity in unit of the light speed, $u_{\rm B}(t) = B^2(t)/8\pi$ is the energy density of the magnetic field, and $w(k, t) = W(k, t)/V(t)$ is the spectral density of the turbulent waves, and $V(t) = 4\pi R^3(t)/3$ is the volume of the nebula. Furthermore, the magnetic field strength in the nebula can be given by (e.g., Y. Zhou & W. H. Matthaeus 1990)

$$B(t) = \left[8\pi \int w_{\rm B}(k, t)dk\right]^{1/2}, \quad (7)$$

where the turbulent magnetic field energy density is assumed to be $w_{\rm B}(k, t) = 0.5w(k, t)$, which is derived from the requirement that the kinetic and magnetic energy densities of the turbulence would be equal (Y. Zhou & W. H. Matthaeus 1990; J. A. Miller et al. 1996).

The Alfvén velocity in the turbulent region can be determined by the magnetic field strength $B(t)$ and the ion density $n_{\rm p}$ as $\nu_{\rm A}(t) = B(t)/\sqrt{4\pi m_{\rm p} n_{\rm p}}$ (e.g., I. Appenzeller et al. 2002). We notice that the proton density in PWNe is also poorly constrained, and a simple estimation is that the density of protons within the nebula is equal to the ratio of the mass in filaments to the volume of the nebula (e.g., P. Slane et al. 2004; P. J. Owen & M. J. Barlow 2015; Z. Cao et al. 2021). However, a PWN is a dynamical nebula, meaning that the proton density in the nebula may vary over time. Thus, in this paper, a typical value of $n_{\rm p} = 0.1\,{\rm cm}^{-3}$ is adopted for simplification (e.g., N. Bucciantini et al. 2011). Such a density may be produced by the neutral particles penetrating into the PWN and being photoionized (S. J. Tanaka & K. Asano 2017).

Assuming the adiabatic losses to be shared equally among all the turbulent waves present in the nebula, the adiabatic loss rate of the turbulent waves can be given by

$$\dot{k}_{\rm ad} = \frac{k}{R(t)}\frac{dR(t)}{dt}. \quad (8)$$

Here, the radius of PWN in the free-expansion phase is calculated with (N. Bucciantini et al. 2011)

$$R(t) = 1.44\left(\frac{E_{\rm sn}^3 L^2(t)}{M_{\rm ej}^5}\right)^{1/10}\left(\frac{t}{1 + t/\tau_0}\right)^{6/5} \times \frac{1}{1 - s}\sum_{i=0}^{\infty} c_i s^i, \quad (9)$$

where $E_{\rm sn}$ is the energy of the supernova explosion, $M_{\rm ej}$ is the mass ejected, and the term $s = (t/\tau_0)/(1 + t/\tau_0)$, and the coefficients c_i can be found in N. Bucciantini et al. (2004).

We now turn to the particle evolution Equation (4), where the function $Q_{\rm e,inj}(\gamma, t)$ represents the injection of the particles. The multiband observations of PWNe have indicated that the injected particles at the TS can be divided into two components: a low-energy component responsible for the radio and GeV emission, and a high-energy component that generates X-ray and TeV γ-rays (e.g., B. M. Gaensler & P. O. Slane 2006; L. Zhang et al. 2008). Meanwhile, the multidimensional particle-in-cell simulations have demonstrated that the spectrum of the injected particles can be fitted as a broken power-law function under certain physical conditions (e.g., L. Sironi & A. Spitkovsky 2011; L. Sironi et al. 2013). As a result, in this paper, a broken power law with different indices and a broken energy spectrum for the injected particles is adopted, that is

$$Q_{\rm e,inj}(\gamma, t) = \begin{cases} Q_{\rm e,0}(t)(\gamma/\gamma_{\rm b})^{-\alpha_1} & \text{for } \gamma < \gamma_{\rm b} \\ Q_{\rm e,0}(t)(\gamma/\gamma_{\rm b})^{-\alpha_2} & \text{for } \gamma \geqslant \gamma_{\rm b} \end{cases}, \quad (10)$$

where α_1 and α_2 are the spectral indices, $\gamma_{\rm b}$ is the break energy, and $Q_{\rm e,0}(t)$ is normalization constant that is determined by $(1 - \eta_{\rm w})L(t) = \int_0^\infty \gamma m_{\rm e} c^2 Q_{\rm e,inj}(\gamma, t)d\gamma$.

It is generally believed that in a stochastic wave-particle system particles will gain energy from turbulent waves via the gyroresonant interactions in the condition of $\omega - k_\parallel v_\parallel - l\Omega_{\rm g} = 0$ ($l = 0, \pm 1, \pm 2, \ldots$), where ω and $k_\parallel$ are, respectively, the frequency and parallel wavenumber of the waves, $v_\parallel$ and $\Omega_{\rm g}$ are the parallel speed and gyrofrequency of the particles, respectively (e.g.,H. Karimabadi et al. 1994, and references therein). The harmonic number l is equal to zero for the resonance with the parallel magnetic field, while $l = \pm 1, \pm 2, \ldots$ for the resonance with the transverse magnetic field. Moreover, the energy gain of particles in the turbulent fields can usually be described as a diffusion process of the particles in the momentum space (e.g., V. S. Ptuskin 1988; I. Appenzeller et al. 2002), i.e., a stochastic acceleration process for the particles (e.g., J. A. Miller & D. A. Roberts

1995; J. A. Miller et al. 1996). In this context, the diffusion nature of the acceleration can be revealed by writing the resulting momentum diffusion equation as a Fokker–Planck equation in the energy space, along with the energy gain rate related to the momentum diffusion coefficient, given by

$$\frac{1}{m_e c^2}\left\langle \frac{dE}{dt}\right\rangle = \frac{1}{p^2}\frac{\partial}{\partial p}[p^2 D_{pp}(p)], \quad (11)$$

where E and p are the energy and momentum of the particles, respectively, and $D_{pp}(p)$ is the momentum diffusion coefficient which represents the rate of the particles interact with the turbulent fields.

In Equation (11), the diffusion coefficients can be readily calculated by using the Hamiltonian approach of H. Karimabadi et al. (1992). Adopting the energy of particle γ instead of its momentum, the diffusion coefficient in the γ-space can then be given by (e.g., J. A. Miller & D. A. Roberts 1995; J. Kakuwa 2016)

$$D_{EE} = \frac{\gamma^2 \beta_w^2(t) k_{res} c}{r_g(\gamma, t) u_B(t)} \int_{k_{res}} \frac{w_B(k, t)}{k} dk, \quad (12)$$

where $r_g(\gamma, t) = \gamma m_e c^2/[eB(t)]$ is the gyroradius of particles with e the charge of the electrons, and $k_{res} = 1/r_g(\gamma, t)$ is the corresponding wavenumber of the turbulent waves resonating with electrons of γ. Moreover, the spatial diffusion coefficient D_{RR} can be calculated with (e.g., J. Skilling 1975)

$$D_{RR} D_{EE} = \frac{1}{9}\nu_A^2(t)\gamma^2. \quad (13)$$

Note that, in Equation (3), we have included a loss term $-\Gamma_k W(k, t)$ for the damping of turbulent waves. Here, we only consider the damping effect due to the gyroresonance of electrons. In this scenario, the energy dissipation rate of the turbulent waves should be equal to the energy gain rate of the electrons (J. A. Eilek & R. N. Henriksen 1984; G. Brunetti & A. Lazarian 2007), that is

$$\int dk \Gamma_k W(k, t) = \int d\gamma \gamma m_e c^2 \partial F_e/\partial\gamma, \quad (14)$$

with

$$\frac{\partial F_e}{\partial \gamma} = \gamma^2 D_{EE}\frac{\partial}{\partial\gamma}\left[\frac{N(\gamma, t)}{\gamma^2}\right]. \quad (15)$$

Then, from Equation (12), performing a partial integration of Equation (14), the damping effect for the turbulent spectrum can be given by (J. Kakuwa 2016)

$$\Gamma_k = \Gamma_k(k, t) = -\frac{4\pi e^2 \beta_w^2(t)}{m_e c k}\int_{\gamma_{res}}^{\infty} d\gamma \gamma^2 \frac{\partial}{\partial\gamma}\left[\frac{n(\gamma, t)}{\gamma^2}\right], \quad (16)$$

where γ_{res} is defined with $\gamma_{res} = \gamma_{res}(k, t) = eB(t)/(m_e c^2 k)$, and $n(\gamma, t) = N(\gamma, t)/V(t)$ represents the number density of the electrons.

Particles will suffer from radiative losses as they are transported within PWNe. In our model, the total energy loss rate of the particles is given by

$$\dot{\gamma} = \dot{\gamma}_{ad} + \dot{\gamma}_{syn} + \dot{\gamma}_{IC}, \quad (17)$$

where $\dot{\gamma}_{ad}$, $\dot{\gamma}_{syn}$, and $\dot{\gamma}_{IC}$ are the energy loss due to adiabatic, synchrotron radiation, and IC scattering processes, respectively. More detailed descriptions of the energy loss rate can be found in J. Martin et al. (2012).

Finally, according to F.-W. Lu et al. (2023b), numerically solving the coupled Equations (3) and (4) simultaneously by using the Crank-Nicolson method, the turbulent wave and electron spectra of the nebula can be obtained. Then, the nonthermal photon emissivity due to synchrotron and IC processes can be calculated using the expressions provided in G.R. Blumenthal & R.J. Gould (1970). In the IC processes, the soft photons from the cosmic microwave background (CMB), the galactic far-infrared (FIR) background, the near-infrared (NIR) and optical photon field due to the stars, and the synchrotron photons (SSC) are taken into account (e.g., C. F. Kennel & F. V. Coroniti 1984b; L. Zhang et al. 2008).

Table 1
Values of the Adopted Physical Parameters for the PWNe 3C58 and G54.1+0.3, Which are Obtained from P. Slane et al. (2004), F. Bocchino et al. (2010), Torres et al. (2013, 2014), H.E.S.S. Collaboration et al. (2018b), and F.-W. Lu et al. (2020), Respectively

Adopted Parameter	Symbol	3C58	G54.1+0.3
Pulsar and ejecta parameters			
SN explosion energy (10^{51} erg)	E_{sn}	1.0	1.0
Ejected mass ($M_\odot$)	M_{ej}	10.0	10.0
ISM density (atoms cm^{-3})	n_{ISM}	0.3	0.2
Period (ms)	P	0.0657	0.136
Period derivative (s s^{-1})	$\dot{P}$	1.93×10^{-13}	7.5×10^{-13}
Current spin-down luminosity (erg s^{-1})	L_{sd}	2.7×10^{37}	1.2×10^{37}
Distance (kpc)	d	2.0	6.2
Background soft photon fields			
CMB temperature (K)	T_{CMB}	2.73	2.73
CMB energy density (eV cm^{-3})	U_{CMB}	0.25	0.25
FIR temperature (K)	T_{FIR}	25	20
FIR energy density (eV cm^{-3})	U_{FIR}	0.1	2.0
NIR temperature (K)	T_{NIR}	2900	3000
NIR energy density (eV cm^{-3})	U_{NIR}	0.5	1.0

3. Modeling Results

In this section, we apply the model to reconstruct the spectral energy distributions (SEDs) of the two Crab-like PWNe, 3C58 and G54.1+0.3. Because the properties of the turbulence within PWNe remain unclear, we employ two classical turbulence models in the nebulae: Kolmogorov-type and Kraichnan-type turbulence, denoted as KO and KR models, respectively.

In fitting the SEDs of these two PWNe, the Markov Chain Monte Carlo (MCMC) method is employed to explore the parameter space (emcee; D. Foreman-Mackey et al. 2013, and references therein). The values of the adopted and fitted physical parameters are listed in Tables 1 and 2, respectively. As we will see in the following, the SEDs of 3C58 and G54.1+0.3 are reproduced, and subsequently the turbulent transport characteristics of the particles within these two PWNe are examined.

3.1. 3C58

Observations indicate that 3C58 is centered on the pulsar PSR J0205+6449 (S. S. Murray et al. 2002) and is located at a distance of $d = 2$ kpc (R. Kothes 2013). The pulsar PSR J0205

Table 2
Values of the Best-fitting Physical Parameters and the Derived Parameters for the PWNe 3C58 and G54.1+0.3 in KO and KR Models

Magnitude	Symbol	3C58		G54.1+0.3	
		KO Model	KR Model	KO Model	KR Model
Fitting parameters					
Initial rotation period (ms)	P_0	$38.11^{+2.02}_{-2.13}$	$42.21^{+1.32}_{-1.45}$	$69.43^{+5.93}_{-5.88}$	$78.48^{+5.98}_{-6.80}$
Braking index	n	$2.80^{+0.14}_{-0.20}$	$1.70^{+0.50}_{-0.29}$	$2.49^{+0.29}_{-0.29}$	$1.95^{+0.71}_{-0.66}$
Turbulent energy fraction (%)	η_w	$37.65^{+7.23}_{-6.17}$	$23.26^{+3.80}_{-3.08}$	$19.30^{+2.93}_{-6.12}$	$8.80^{+2.49}_{-1.65}$
Low-energy electron index	α_1	$0.61^{+0.10}_{-0.11}$	$0.83^{+0.07}_{-0.09}$	$1.19^{+0.11}_{-0.11}$	$1.36^{+0.14}_{-0.13}$
High-energy electron index	α_2	$2.92^{+0.01}_{-0.01}$	$2.92^{+0.01}_{-0.01}$	$2.65^{+0.03}_{-0.03}$	$2.63^{+0.03}_{-0.03}$
Break energy of electrons	$\log_{10}\gamma_b$	$4.86^{+0.04}_{-0.04}$	$4.75^{+0.03}_{-0.03}$	$5.77^{+0.11}_{-0.11}$	$5.69^{+0.13}_{-0.15}$
Maximum energy of electrons	$\log_{10}\gamma_{max}$	$\geqslant 9.67$	$\geqslant 9.72$	$\geqslant 9.46$	$\geqslant 9.58$
Derived parameters					
Age of the pulsar (yr)	T_{age}	3663	4107	2442	2463
Spin-down timescale (yr)	τ_0	2724	11313	1417	3590
Current magnetic field (μG)	$B(T_{age})$	16.3	16.4	15.6	15.1
Current alfvén velocity (km s^{-1})	$\nu_A(T_{age})$	113	113	107	104

+6449 has a rotational period of $P = 65.7$ ms, a period derivative of $\dot{P} = 1.93 \times 10^{-13}$ s s^{-1}, a characteristic age of $\tau_c = 5397$ yr, and a current spin-down luminosity of $L_{sd} = 2.7 \times 10^{37}$ erg s^{-1} (e.g., S. S. Murray et al. 2002; M. A. Livingstone et al. 2009). The braking index and initial rotation period of PSR J0205+ 6449 are uncertain, so we treat them as fitting parameters, where the initial rotation period is mainly used to determine the age of the pulsar via Equation (2).

As one of the well-known PWNe, the morphology of 3C58 has been found to be similar to the Crab Nebula, and the photon emission from the nebula has been detected in radio, infrared (IR), X-ray, and GeV and TeV γ-ray bands. To reconstruct the multiband photon spectrum of the PWN, we acquired the observations of 3C58 as follows: D. A. Green (1986), H. W. Morsi & W. Reich (1987), C. J. Salter et al. (1989), and Planck Collaboration et al. (2016) for the radio band; P. Slane et al. (2008) for the IR band; K. Torii et al. (2000) and H. An (2019) for the X-ray band; A. A. Abdo et al. (2013), M. Ackermann et al. (2013), and J. Aleksić et al. (2014) for the GeV and TeV γ-ray bands.

Figure 1 shows the fitting results for KO and KR models of the SEDs of 3C58, indicating that the SEDs of 3C58 can be well reproduced by both KO and KR models. The evolution of the Alfvén velocity, which plays an important role in the energy cascade process of the turbulent waves, is shown in Figure 2, revealing that the Alfvén velocity decreases with the increase of time, and the current Alfvén velocity has a value of 113 km s^{-1} in both KO and KR models.

With the fitting parameters listed in Table 2, it can be found that the braking index and age of the pulsar are significantly different in these two models, i.e., the braking index of the pulsar is estimated to be 2.80 in KO model but 1.70 in KR model, and the age of the pulsar is 3663 yr in KO model while 4107 yr in KR model. Moreover, KO model allows a fraction of 37.65% spin-down energy to be converted into turbulent energy, but in KR model, a fraction of 23.26% is required. Consequently, according to Equation (7), the current magnetic field of 3C58 can be obtained to be 16.3 μG and 16.4 μG in the Kolmogorov- and Kraichnan-type turbulence, respectively. The magnetic fields obtained in our models are consistent with the value of 15.6 μG estimated by J. Martin & D. F. Torres (2022), but smaller than the value of $\sim$30 μG obtained by D. F. Torres et al. (2013) and B.-T. Zhu et al. (2021), due to the NuSTAR X-ray observations given by H. An (2019) were considered in our calculations.

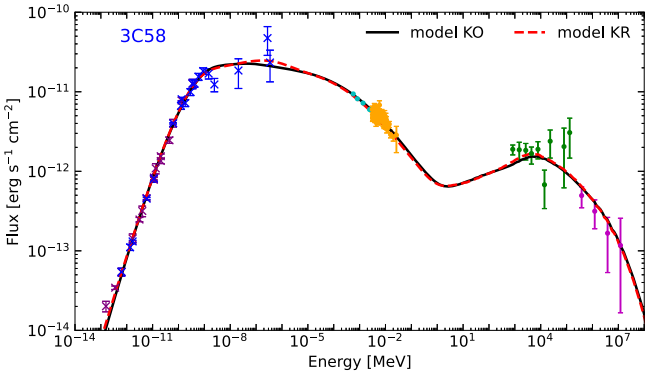

Figure 1. Fitting results of the SEDs of 3C58 in KO (black-solid line) and KR (red-dashed line) models.

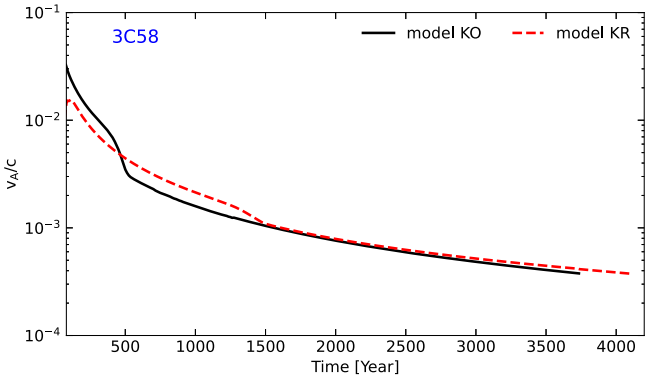

Figure 2. The evolution of the Alfvén speed for 3C58 in KO (black-solid line) and KR (red-dashed line) models.

Particularly, the spectral indices of low-energy injection electrons differ significantly between KO and KR models; that is, $\alpha_1 = 0.61$ in KO model and $\alpha_1 = 0.83$ in KR model. These differences in parameter values can be attributed to the different types of turbulence that are considered in these two models. The efficiencies of the energy exchange between the waves and

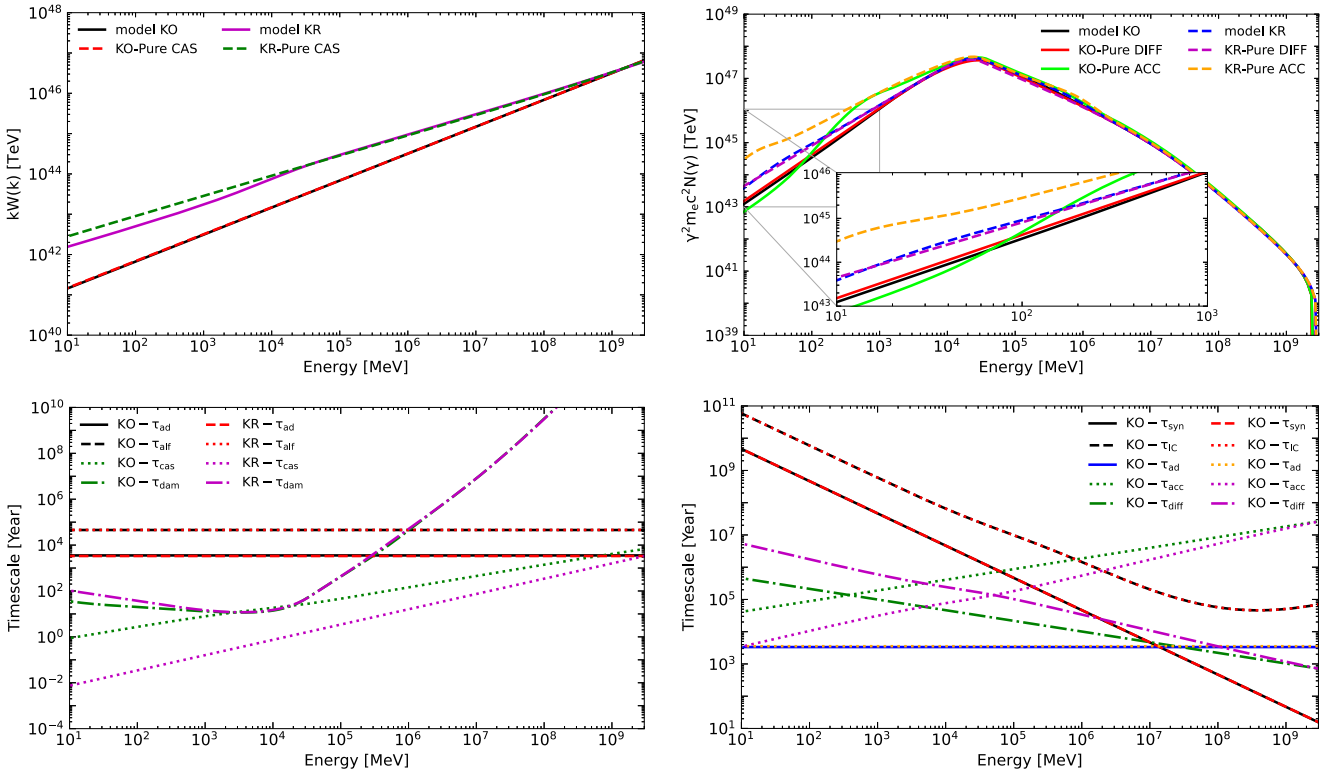

Figure 3. Top panels: the current spectral distributions of the turbulent waves (left) and electrons (right) of 3C58 calculated in the framework of KO and KR models, respectively. Bottom panels: the current timescales of the turbulent waves (left) and electrons (right) of 3C58. The spectra and timescales for the turbulent waves with wavenumber k are plotted at the resonant energy of $E_{\rm res}(k) = eB/k$ for the convenience of discussions.

particles differ significantly in Kolmogorov- and Kraichnan-type turbulence (e.g., J. Cho & A. Lazarian 2002), resulting in differences in the effects of the stochastic acceleration and spatial diffusion processes on the electron spectrum, and thus differences in the fitting parameter values.

It should be noted that the maximum energy of the particles within 3C58 can only be constrained to a lower value by the turbulent diffusion model; that is, the lower limit of the maximum energy of particles within 3C58 is estimated to be 2.4 PeV and 2.7 PeV in KO and KR models, respectively. This is because when the maximum energy of the particles is up to an appropriate value, the increases in the maximum energy will not significantly alter the particle spectrum, due to the impact of the synchrotron radiation and IC scattering cooling losses on the evolution of the high-energy particles (e.g., J. Martin & D. F. Torres 2022). These estimations of the maximum energy of the particles are consistent with the result of 3.7 PeV obtained by D. F. Torres et al. (2013) with a Bohm diffusion model and the value of 2.0 PeV given by B.-T. Zhu et al. (2021) with a parameterized Kolmogorov turbulent diffusion model.

We also show the calculated results of the current turbulent and electron spectra, as well as the corresponding timescales, in Figure 3, where the spectra and timescales for the turbulent waves with wavenumber k are plotted at the resonant energy of $E_{\rm res}(k) = eB/k$ for the sake of discussion. In the calculations, except for the Alfvén crossing time $\tau_{\rm alf} = R(t)/\nu_{\rm A}(t)$, the other timescales of the turbulent waves are determined with

$$\tau_{\rm ad} = \left[\frac{1}{R(t)}\frac{dR(t)}{dt}\right]^{-1}, \tag{18}$$

$$\tau_{\rm cas} = \begin{cases} \dfrac{1}{k\beta_{\rm w}(t)c}\left[\dfrac{2u_{\rm B}(t)}{kw(k,\,t)}\right]^{1/2} & \text{(Kolmogorov)} \\ \dfrac{1}{k\beta_{\rm w}(t)c}\left[\dfrac{2u_{\rm B}(t)}{kw(k,\,t)}\right] & \text{(Kraichnan)} \end{cases}, \tag{19}$$

and

$$\tau_{\rm dam} = \left\{-\frac{4\pi e^2\beta_{\rm w}^2(t)}{m_{\rm e}ck}\int_{\gamma_{\rm res}}^{\infty} d\gamma\gamma^2\frac{\partial}{\partial\gamma}\left[\frac{n(\gamma,\,t)}{\gamma^2}\right]\right\}^{-1}, \tag{20}$$

where $\tau_{\rm ad}$, $\tau_{\rm cas}$, and $\tau_{\rm dam}$ are the timescales of adiabatic, energy cascade and damping processes, respectively. Meanwhile, except for the adiabatic loss timescale calculated with Equation (18), the timescales of acceleration $\tau_{\rm acc}$, spatial diffusion $\tau_{\rm diff}$, synchrotron $\tau_{\rm syn}$ and IC scattering $\tau_{\rm IC}$ processes of electrons are respectively given by

$$\tau_{\rm acc} = \left[\frac{\beta_{\rm w}^2 k_{\rm res}c}{r_{\rm g}(\gamma,\,t)u_{\rm B}(t)}\int_{k_{\rm res}}\frac{w_{\rm B}(k,\,t)}{k}dk\right]^{-1}, \tag{21}$$

$$\tau_{\rm diff} = \frac{R^2(t)}{D_{\rm RR}} = \frac{9R^2(t)}{\nu_{\rm A}^2(t)\tau_{\rm acc}}, \tag{22}$$

$$\tau_{\rm syn} = \frac{3m_{\rm e}c}{4\sigma_{\rm T}\gamma}\frac{1}{u_{\rm B}(t)}, \tag{23}$$

and

$$\tau_{\rm IC} = \frac{\pi^4 m_{\rm e}c}{20\sigma_{\rm T}\gamma}\frac{1}{U_{\rm ph}Y(\gamma,\,T)}, \tag{24}$$

where σ_T is the Thomson cross section, T and U_{ph} are the temperature and energy density of the graybody photon field, respectively, and the detailed expression of the function $Y(\gamma, T)$ can be found in K. Fang et al. (2021).

The Alfvén velocity can play an important role in energy cascade process of the turbulent waves, but the Alfvén crossing time appears to play a much smaller role in the evolution of turbulent waves, due to $\tau_{alf} \gg \tau_{ad}$ as the timescales displayed in the left-bottom panel of Figure 3. In the wave-particle systems, on the other hand, the processes of energy cascade and damping could play a role in changing the distribution of the turbulent waves, whereas the processes of stochastic acceleration and spatial diffusion escape may be important for modulating the electron spectrum (e.g., J. A. Miller et al. 1996; F.-W. Lu et al. 2023b). Therefore, we calculate the turbulent wave and electron spectra in the following three scenarios:

(1) Pure CAS: The energy cascade process for turbulent waves is considered, while the damping process is not, and that both the stochastic acceleration and spatial diffusion escape processes for electrons are included.

(2) Pure ACC: For electrons, the stochastic acceleration process is considered, but the spatial diffusion escape process is not. Additionally, both the energy cascade and damping processes for turbulent waves are taken into account.

(3) Pure DIFF: The stochastic acceleration process is neglected, while the spatial diffusion escape process is considered for electrons. Meanwhile, both the energy cascade and damping processes for turbulent waves are included.

The results of KO and KR models, as well as the results calculated in the above-mentioned three scenarios, are shown in the top panels of Figure 3. It should be noted that both the spectra and timescales of the turbulent waves and electrons are calculated as of the present day. Therefore, the modeling results shown in Figure 3 can only reflect the current effects of the physical processes on the turbulent and electron spectra.

Damping occurs when particles gain energy from the turbulent waves via the stochastic acceleration process in the wave-particle systems. Thus, it is expected that the damping process is important for changing the shape of the turbulence spectrum (e.g., J. A. Miller et al. 1996). Meanwhile, the energy cascade process is expected to be mainly responsible for transferring the turbulence at a low wavenumber to a higher wavenumber via the wave-wave interactions (F.-W. Lu et al. 2023b). Substituting the diffusion coefficient of Equation (6) in the evolution Equation (3) of the turbulent waves, and assuming a steady sate with no damping, one can obtain $W(k) \propto k^{-q}$, with $q = 5/3$ for the Kolmogorov phenomenology and $q = 3/2$ for the Kraichnan case (J. A. Miller & D. A. Roberts 1995), indicating the spectral index of the turbulent waves is primarily determined by the phenomenology of the cascading turbulence. Furthermore, in combination with the current timescales of turbulent waves and electrons, it can be found the following:

1. In KO model, the energy cascade process dominates over the damping effect for the turbulent waves, implying the energy exchange between waves and particles within the nebula is not very efficient. As a result, the damping process has little effect on the turbulence spectrum, and the distribution of the turbulent waves satisfies $W(k) \propto k^{-5/3}$. Meanwhile, the stochastic acceleration and spatial diffusion processes appear to have some effects on the electron spectrum at the low energies of $E_e \lesssim 0.1$ TeV, but become less effective for the distribution of the electron spectrum at $E_e \gtrsim 0.1$ TeV, due to the evolution of the particles has been gradually translated into synchrotron radiative cooling dominant.
2. In KR model, the damping process seems to be comparable to the energy cascade process at $E_{res}(k) \lesssim 1$ TeV, indicating the energy exchange between the waves and the particles is very efficient. This result in the turbulent spectrum that does not follow a linear distribution at the low resonant energies. However, with $E_{res}(k) \gtrsim 1$ TeV, the energy cascade process seems to be more effective, leading to the distribution of the turbulent waves that satisfies $W(k) \propto k^{-3/2}$. For the electrons, the spatial diffusion escape process dominates over the acceleration process, and it is more important for modifying the electron spectrum at $E_e \lesssim 1$ TeV. Whereas at $E_e \gtrsim 1$ TeV, the synchrotron radiative cooling loss seems to dominate over both the acceleration and spatial diffusion processes, leading to the stochastic acceleration and spatial diffusion processes seem not to be very effective for the electron spectrum.

Above all, in Kolmogorov-type turbulence, the acceleration and spatial diffusion processes appear less effective for the evolution of the particle spectrum of 3C58, while in Kraichnan-type turbulence, the spatial diffusion process plays an important role in the modulating the particle spectrum at low energies. This is due to the differences in the efficiencies of energy exchange between the turbulent waves and particles in Kolmogorov- and Kraichnan-type turbulence.

3.2. G54.1+0.3

PWN G54.1+0.3 is generally believed to be powered by the center pulsar PSR J1930+1852. The pulsar PSR J1930+1852 has a rotation period of $P = 136$ ms, a period derivative of $\dot{P} = 7.5 \times 10^{-13}$ s s^{-1}, a characteristic age of $\tau_c = 2871$ yr, and a current spin-down luminosity of $L_{sd} = 1.2 \times 10^{37}$ erg s^{-1} (F. Camilo et al. 2002). Based on HI absorption and morphological association with a CO molecular cloud, the distance from Earth to the PWN has been estimated to be $d = 6.2^{+1.0}_{-0.6}$ kpc (D. A. Leahy et al. 2008).

As one of the other famous Crab-like PWNe, G54.1+0.3 has also been observed in radio, X-ray, and TeV γ-ray bands. To perform the fitting of the SEDs of G54.1+0.3, the observations of the PWN are collected as follows: radio data are obtained from N. Hurley-Walker et al. (2009) and C. C. Lang et al. (2010), X-ray data are taken from F. J. Lu et al. (2001, 2002), and γ-ray data are obtained from V. A. Acciari et al. (2010) and A. U. Abeysekara et al. (2018).

With the parameters listed in Tables 1 and 2, we obtain the SEDs and the evolution of the Alfvén velocity of G54.1+0.3 in framework of the KO and KR models in Figures 4 and 5. Correspondingly, the electron and turbulent wave spectra, as well as the timescales, are shown in Figure 6. Both the KO and KR models can accurately reproduce the SEDs of G54.1+0.3, and the Alfvén velocity is found to decrease with the increase of time.

The fitting parameters in the KO model are different from those in the KR model, especially regarding the fraction of the spin-down energy to be converted into turbulent energy and the

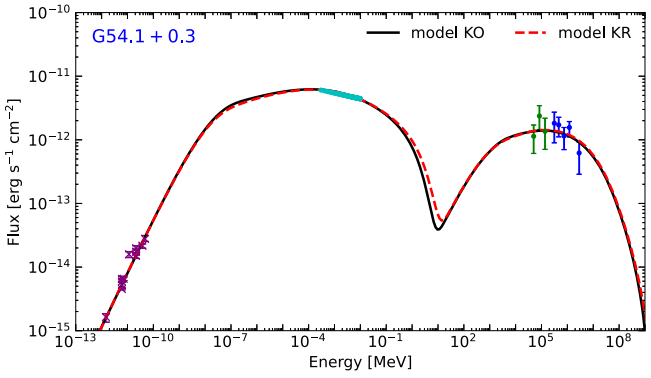

Figure 4. Fitting results of the SEDs of G54.1+0.3 in KO (black-solid line) and KR (red-dashed line) models.

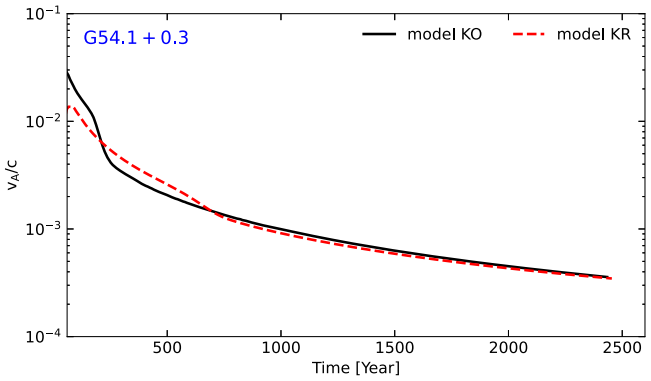

Figure 5. The evolution of the Alfvén speed for G54.1+0.3 in KO (black-solid line) and KR (red-dashed line) models.

spectral index of the low-energy injection electrons (see Table 2). From the modeling results, it can be found that the braking index of the pulsar has a value of 2.48 in the KO model but has a value of 1.95 in the KR model. The current Alfvén velocity of turbulent waves within G54.1+0.3 is predicted to be 107 km s^{-1} and 104 km s^{-1} in the KO and KR models, respectively, closing to the value of 113 km s^{-1} of the waves within 3C58. Meanwhile, the current magnetic field strengths are obtained as 15.6 μG and 15.1 μG in the KO and KR models, respectively. Moreover, the lower limits of maximum energy of the particles within G54.1+0.3 are, respectively, obtained to be 1.5 PeV and 1.9 PeV in the KO and KR models, which are greater than the value of ∼500 TeV obtained by D. F. Torres et al. (2014) and B.-T. Zhu et al. (2021), due to different treatments of particle diffusion transport.

In Kolmogorov-type turbulence, the damping process plays only a modest role in changing the turbulence spectrum, and the acceleration and spatial diffusion processes exert only minor influences on the electron spectrum at the low energies of $E_e \lesssim 0.5$ TeV. Whereas, in Kraichnan-type turbulence, the damping process appears to be more effective, i.e., the energy exchange between the turbulent waves and particles is more efficient, leading to the damping effect reducing the intensity of the turbulent spectrum, and subsequently causing the spatial diffusion process to modulate the electron spectrum at energies of $E_e \lesssim 1.0$ TeV. Note that, at high energies of $E_e \gtrsim 1.0$ TeV, stochastic acceleration and spatial diffusion processes appear to not be very effective in both Kolmogorov- and Kraichnan-type turbulence, since the synchrotron cooling dominates the evolution of the particles.

Therefore, for G54.1+0.3, the evolution of the particle spectrum in Kolmogorov-type turbulence is somewhat influenced by the stochastic acceleration and spatial diffusion processes, while in Kraichnan-type turbulence the spatial diffusion process plays a more important role in modulating the particle spectrum at low energies. These findings resemble the modeling results that appeared in 3C58.

Finally, based on the parameter space of the maximum energy of the particles explored by using the MCMC method, it can be found that electrons within 3C58 and G54.1+0.3 may have been accelerated to PeV energies, implying that these two Crab-like PWNe are possibly the electron PeVatrons in the Galaxy.

3.3. Turbulent Transport Characteristics

Once the distribution of the turbulent waves is determined, the energy and spatial diffusion coefficients can be obtained via Equations (12) and (13). Thus, in this section, the turbulent transport characteristics of the particles within 3C58 and G54.1+0.3 are investigated in the framework of the KO and KR models. In Figure 7, the current distributions of the energy and spatial diffusion coefficients for 3C58 and G54.1+0.3 predicted by the KO and KR models are shown. Moreover, the predicted results of the Crab Nebula obtained by F.-W. Lu et al. (2023b) are also displayed in the figure for comparison.

The current energy and spatial diffusion coefficients of 3C58 and G54.1+0.3 appear to follow nonlinear distributions in Kraichnan-type turbulence, while they follow quasi-linear distributions in Kolmogorov-type turbulence at low energies. From Equations (12) and (13), the energy and spatial diffusion coefficients can be approximated to be $D_{EE} \propto \gamma k_{res} w(k_{res})$ and $D_{RR} \propto \gamma/[k_{res} w(k_{res})]$ (e.g., J. Kakuwa 2016; F.-W. Lu et al. 2023b). Therefore, as demonstrated in Sections 3.1 and 3.2, quasi-linear (nonlinear) distributions of the energy and spatial diffusion coefficients in the Kolmogorov (Kraichnan) turbulence can be attributed to the effects of the damping process on the turbulent spectrum.

At high energies of $E_e \geqslant 1$ TeV, both the predicted energy and spatial diffusion coefficients seem to follow linear distributions, since the evolution of the turbulent spectrum is energy cascade dominated. Note that the turbulent spectrum in the energy cascade dominant case would be satisfied $W(k) \propto k^{-q}$, with $q = 5/3$ for the Kolmogorov-type turbulence and $q = 3/2$ for the Kraichnan-type turbulence (J. A. Miller et al. 1996). Consequently, at high energies of $E_e \geqslant 1$ TeV, the energy and spatial diffusion coefficients can be obtained to be $D_{EE} \propto E_e^{5/3}$ and $D_{RR} \propto E_e^{1/3}$ for the Kolmogorov-type turbulence and $D_{EE} \propto E_e^{3/2}$ and $D_{RR} \propto E_e^{1/2}$ for the Kraichnan-type turbulence. Thus, linear distributions of the energy and spatial diffusion coefficients are expected at high energies.

These modeling results of the distributions of the diffusion coefficients of 3C58 and G54.1+0.3 are incredibly comparable to the results of the Crab Nebula obtained by F.-W. Lu et al. (2023b) (see Figure 7). Moreover, by fitting the energy and spatial diffusion coefficients with the power-law functions at the high energies of $E_e \geqslant 1$ TeV, i.e., $D_{EE} = D_{0,EE}(E_e/1\ \mathrm{TeV})^{\delta_{EE}}$ and $D_{RR} = D_{0,RR}(E_e/1\ \mathrm{TeV})^{\delta_{RR}}$, it can be found that the current spatial diffusion coefficients at an electron energy of 1 TeV are about two orders of magnitude smaller than the standard diffusion coefficient in the ISM (e.g., A. W. Strong et al. 2007; M. Aguilar et al. 2016) in both the Kolmogorov- and Kraichnan-type turbulence, as shown in the fitting parameters listed in

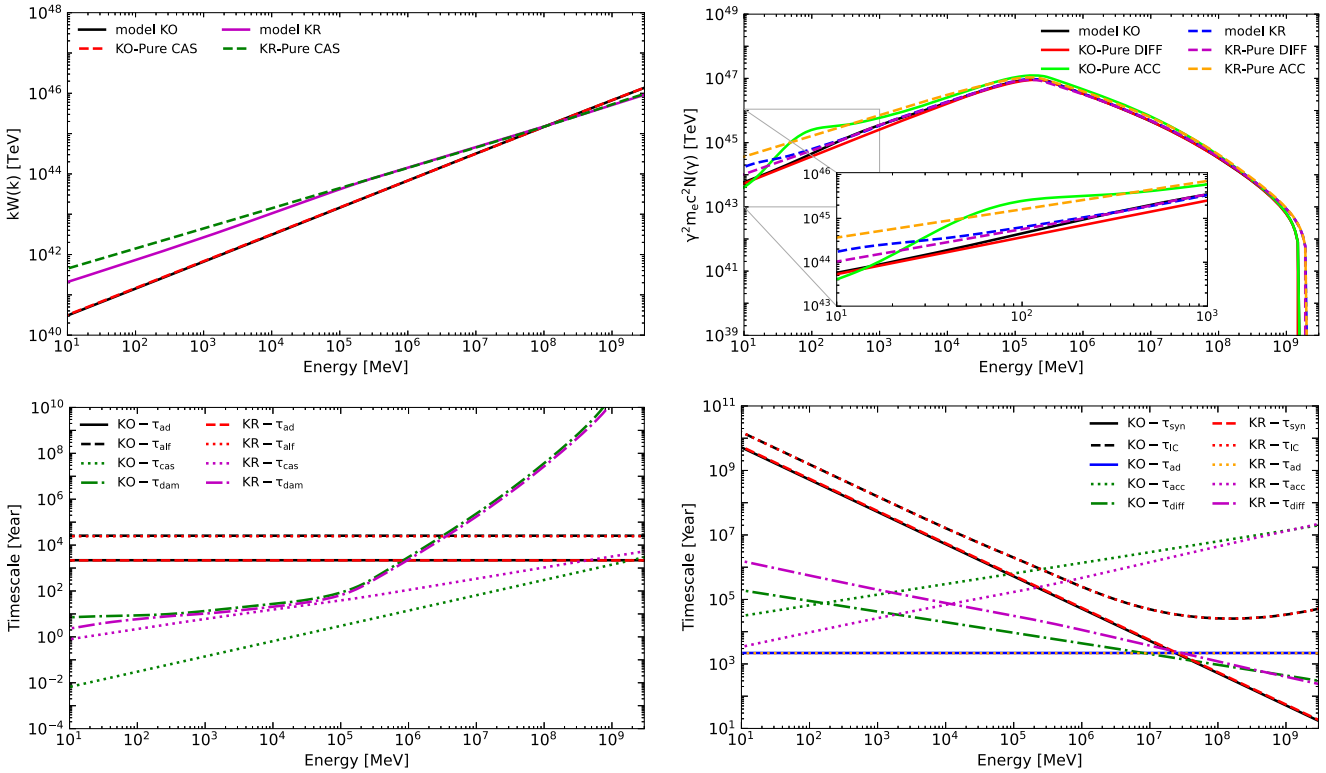

Figure 6. Top panels: The current spectral distributions of the turbulent waves (left-hand panel) and electrons (right-hand panel) of G54.1+0.3 calculated in the framework of KO and KR models, respectively. Bottom panels: The current timescales of the turbulent waves (left-hand panel) and electrons (right-hand panel) of G54.1+0.3.

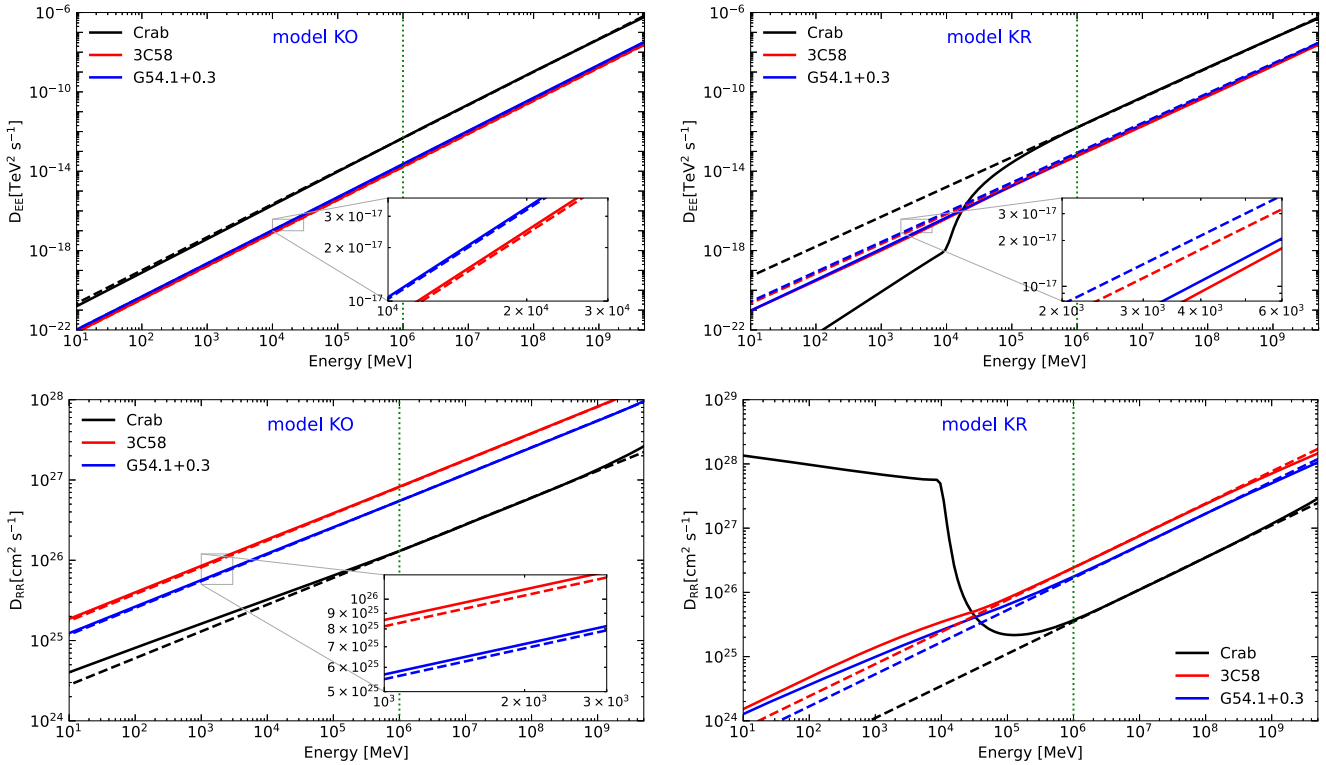

Figure 7. Left-hand panels: The current distributions of the energy (top panel) and spatial (bottom panel) diffusion coefficients obtained in the KO model for the Crab Nebula (black line), 3C58 (red line), and G54.1+0.3 (blue line). Right-hand panels: Same as the left-hand panels but for the KR model. Corresponding dashed lines shown in the top and bottom panels are the fitting results for the power-law fits with indices of 5/3 (3/2) for the energy diffusion coefficient and 1/3 (1/2) for the spatial diffusion coefficient in the Kolmogorov (Kraichnan) turbulence at $E_e \geqslant 1$ TeV.

Table 3
Power-law Fitting Parameters for the Energy and Spatial Diffusion Coefficients at $E_e \geqslant 1$ TeV in the Kolmogorov- and Kraichnan-type Turbulence, Respectively, with $D_{EE} = D_{0,EE}(E_e/1\ \mathrm{TeV})^{\delta_{EE}}$ and $D_{RR} = D_{0,RR}(E_e/1\ \mathrm{TeV})^{\delta_{RR}}$

Symbol	3C58		G54.1+0.3		Crab Nebula	
	KO Model	KR Model	KO Model	KR Model	KO Model	KR Model
$D_{0,EE}$ [TeV^2 s^{-1}]	2.2×10^{-14}	6.9×10^{-14}	3.0×10^{-14}	8.3×10^{-14}	6.4×10^{-13}	1.6×10^{-12}
δ_{EE}	5/3	3/2	5/3	3/2	5/3	3/2
$D_{0,RR}$ [cm^2 s^{-1}]	8.2×10^{26}	2.4×10^{26}	5.5×10^{26}	1.7×10^{26}	1.3×10^{26}	3.5×10^{25}
δ_{RR}	1/3	1/2	1/3	1/2	1/3	1/2

Table 3. This implies that a common slow diffusion escape may occur in the PWNe Crab Nebula, 3C58, and G54.1+0.3, consistent with the results predicted by B.-T. Zhu et al. (2021) with their parameterized diffusion model.

4. Discussion and Conclusions

In this paper, a turbulent diffusion model proposed by F.-W. Lu et al. (2023b) is used to investigate the turbulent transport characteristics of particles within two Crab-like PWNe, 3C58 and G54.1+0.3. This turbulent diffusion model can enable us to self-consistently determine the energy and spatial coefficients of particles within PWNe based on the distributions of turbulent waves.

The fitting results of the SEDs of 3C58 and G54.1+0.3 in both Kraichnan- and Kolmogorov-type turbulence are shown in Figures 1 and 4, respectively, demonstrating that the multiband photon emission from these two Crab-like PWNe can be well reproduced. In Kolmogorov-type turbulence, the current stochastic acceleration and spatial escape processes may have some effects on the distributions of the electron spectra, while in Kraichnan-type turbulence the damping process for the turbulent waves appears to be very effective, leading to the spatial diffusion escape of the electrons being more critical for modifying the electron spectrum at low energies (see Figures 3 and 6). These modeling results for 3C58 and G54.1+0.3 are similar to those of the Crab Nebula obtained by F.-W. Lu et al. (2023b). Moreover, as pointed out by Lhaaso Collaboration et al. (2021) and Z. Cao et al. (2021), Crab Nebula is an electron PeVatron in Galaxy. From our calculation, it is expected that electrons within 3C58 and G54.1+0.3 may have been accelerated to PeV energies (see Table 2), and we hypothesize that these two Crab-like PWNe are also electron Pevatrons.

With the distributions of the turbulent waves determined by the fitting of the SEDs of 3C58 and G54.1+0.3, we obtained the energy and spatial diffusion coefficients of the particles within these two Crab-like PWNe, as shown in Figure 7. The distributions of the current energy and spatial diffusion coefficients of electrons are found to follow quasi-linear (nonlinear) functions with energy in the Kolmogorov (Kraichnan) turbulence at $E_e \leqslant 1$ TeV, as a result of the effect of the damping process on the turbulent spectrum, consistent with the suggestions of A. U. Abeysekara et al. (2017). It should be noted that the energy and spatial diffusion coefficients appear to follow linear distributions at $E_e \geqslant 1$ TeV because the energy cascade process of turbulent waves dominates over the damping process at $E_{res} \geqslant 1$ TeV. In particular, our modeling results predicted that the current spatial diffusion coefficients of 3C58 and G54.1+0.3 in Kolmogorov- and Kraichnan-type turbulence are two orders of magnitude smaller than the standard diffusion coefficient in the ISM, implying that a common slow diffusion may occur within these two Crab-like PWNe.

Finally, although our model can enable us to understand the distributions of the current energy and spatial diffusion coefficients of 3C58 and G54.1+0.3, the specific properties of the turbulence in the nebulae remain indistinguishable. Therefore, a spatially dependent turbulent diffusion model should be developed to examine the diffusion transport characteristics of the particles within PWNe more precisely.

Acknowledgments

We thank the anonymous referee for the very constructive comments. L.Z. is partially supported by the National Natural Science Foundation of China (NSFC) under grant 12233006. F.W.L. is partially supported by NSFC under grant 12363006, Yunnan Fundamental Research Projects (No. 202201AT070234), and the Xingdian Talent Support Program of Yunnan Province. B.T.Z. is partially supported by NSFC under grant 12363007. W.H. is supported by NSFC under grant 12263003.

ORCID iDs

Wen Hu https://orcid.org/0000-0003-0429-8636
Li Zhang https://orcid.org/0000-0002-7824-4289

References

Abdalla, H., Aharonian, F., Ait Benkhali, F., et al. 2020, NatAs, 4, 167
Abdo, A. A., Ajello, M., Allafort, A., et al. 2013, ApJS, 208, 17
Abeysekara, A. U., Albert, A., Alfaro, R., et al. 2017, Sci, 358, 911
Abeysekara, A. U., Archer, A., Benbow, W., et al. 2018, ApJ, 866, 24
Acciari, V. A., Aliu, E., Arlen, T., et al. 2010, ApJL, 719, L69
Ackermann, M., Ajello, M., Allafort, A., et al. 2013, ApJS, 209, 34
Aguilar, M., Ali Cavasonza, L., Ambrosi, G., et al. 2016, PhRvL, 117, 231102
Aharonian, F., Akhperjanian, A., Beilicke, M., et al. 2004, ApJ, 614, 897
Aleksić, J., Ansoldi, S., Antonelli, L. A., et al. 2014, A&A, 567, L8
An, H. 2019, ApJ, 876, 150
Appenzeller, I., Borner, G., Dopita, M. A., et al. 2002, Cosmic Ray Astrophysics (Berlin: Springer)
Atoyan, A. M., & Aharonian, F. A. 1996, MNRAS, 278, 525
Blumenthal, G. R., & Gould, R. J. 1970, RvMP, 42, 237
Bocchino, F., Bandiera, R., & Gelfand, J. 2010, A&A, 520, A71
Brunetti, G., & Lazarian, A. 2007, MNRAS, 378, 245
Bucciantini, N., Arons, J., & Amato, E. 2011, MNRAS, 410, 381
Bucciantini, N., Bandiera, R., Blondin, J. M., Amato, E., & Del Zanna, L. 2004, A&A, 422, 609
Caballero-Lopez, R. A., Moraal, H., McCracken, K. G., & McDonald, F. B. 2004, JGRA, 109, A12102
Camilo, F., Lorimer, D. R., Bhat, N. D. R., et al. 2002, ApJL, 574, L71
Cao, Z., Aharonian, F., An, Q., et al. 2024, ApJS, 271, 25
Cao, Z., Aharonian, F. A., An, Q., et al. 2021, Natur, 594, 33
Cho, J., & Lazarian, A. 2002, PhRvL, 88, 245001
Cho, J., & Lazarian, A. 2003, MNRAS, 345, 325
de Jager, O. C., & Harding, A. K. 1992, ApJ, 396, 161
Eilek, J. A., & Henriksen, R. N. 1984, ApJ, 277, 820
Fang, K., Bi, X.-J., Lin, S.-J., & Yuan, Q. 2021, ChPhL, 38, 039801
Fang, K., Bi, X.-J., & Yin, P.-F. 2019, MNRAS, 488, 4074

Foreman-Mackey, D., Hogg, D. W., Lang, D., & Goodman, J. 2013, PASP, 125, 306
Gaensler, B. M., & Slane, P. O. 2006, ARA&A, 44, 17
Goldreich, P., & Julian, W. H. 1969, ApJ, 157, 869
Green, D. A. 1986, MNRAS, 218, 533
H.E.S.S. Collaboration, Abdalla, H., Abramowski, A., et al. 2018a, A&A, 612, A1
H.E.S.S. Collaboration, Abdalla, H., Abramowski, A., et al. 2018b, A&A, 612, A2
Hurley-Walker, N., Scaife, A. M. M., Green, D. A., et al. 2009, MNRAS, 396, 365
Kakuwa, J. 2016, ApJ, 816, 24
Karimabadi, H., Krauss-Varban, D., & Terasawa, T. 1992, JGR, 97, 13853
Karimabadi, H., Omidi, N., & Gary, S. P. 1994, GMS, 84, 221
Kennel, C. F., & Coroniti, F. V. 1984a, ApJ, 283, 694
Kennel, C. F., & Coroniti, F. V. 1984b, ApJ, 283, 710
Kolmogorov, A. 1941, DoSSR, 30, 301
Kothes, R. 2013, A&A, 560, A18
Kraichnan, R. H. 1965, PhFl, 8, 1385
Lang, C. C., Wang, Q. D., Lu, F., & Clubb, K. I. 2010, ApJ, 709, 1125
Leahy, D. A., Tian, W., & Wang, Q. D. 2008, AJ, 136, 1477
Lerche, I., & Schlickeiser, R. 1981, ApJS, 47, 33
LHAASO Collaboration, Cao, Z., Aharonian, F., et al. 2021, Sci, 373, 425
Liu, R.-Y., & Yan, H. 2020, MNRAS, 494, 2618
Livingstone, M. A., Ransom, S. M., Camilo, F., et al. 2009, ApJ, 706, 1163
Lu, F. J., Aschenbach, B., & Song, L. M. 2001, A&A, 370, 570
Lu, F. J., Wang, Q. D., Aschenbach, B., Durouchoux, P., & Song, L. M. 2002, ApJL, 568, L49
Lu, F.-W., Gao, Q.-G., & Zhang, L. 2017, ApJ, 834, 43
Lu, F.-W., Gao, Q.-G., & Zhang, L. 2020, MNRAS, 498, 1911
Lu, F.-W., Zhu, B.-T., Hu, W., & Zhang, L. 2023a, MNRAS, 518, 3949
Lu, F.-W., Zhu, B.-T., Hu, W., & Zhang, L. 2023b, ApJ, 953, 116
Martin, J., & Torres, D. F. 2022, JHEAp, 36, 128
Martin, J., Torres, D. F., & Rea, N. 2012, MNRAS, 427, 415
Miller, J. A., Larosa, T. N., & Moore, R. L. 1996, ApJ, 461, 445
Miller, J. A., & Roberts, D. A. 1995, ApJ, 452, 912
Morsi, H. W., & Reich, W. 1987, A&AS, 69, 533
Murray, S. S., Slane, P. O., Seward, F. D., Ransom, S. M., & Gaensler, B. M. 2002, ApJ, 568, 226
Owen, P. J., & Barlow, M. J. 2015, ApJ, 801, 141
Pacini, F., & Salvati, M. 1973, ApJ, 186, 249
Planck Collaboration, Arnaud, M., Ashdown, M., et al. 2016, A&A, 586, A134
Porth, O., Komissarov, S. S., & Keppens, R. 2014, MNRAS, 438, 278
Porth, O., Vorster, M. J., Lyutikov, M., & Engelbrecht, N. E. 2016, MNRAS, 460, 4135
Ptuskin, V. S. 1988, SvAL, 14, 255
Reich, W., Fuerst, E., Altenhoff, W. J., Reich, P., & Junkes, N. 1985, A&A, 151, L10
Reynolds, S. P., & Chevalier, R. A. 1984, ApJ, 278, 630
Salter, C. J., Reynolds, S. P., Hogg, D. E., Payne, J. M., & Rhodes, P. J. 1989, ApJ, 338, 171
Sironi, L., & Spitkovsky, A. 2011, ApJ, 741, 39
Sironi, L., Spitkovsky, A., & Arons, J. 2013, ApJ, 771, 54
Skilling, J. 1975, MNRAS, 172, 557
Slane, P., Helfand, D. J., Reynolds, S. P., et al. 2008, ApJL, 676, L33
Slane, P., Helfand, D. J., van der Swaluw, E., & Murray, S. S. 2004, ApJ, 616, 403
Strong, A. W., Moskalenko, I. V., & Ptuskin, V. S. 2007, ARNPS, 57, 285
Tanaka, S. J., & Asano, K. 2017, ApJ, 841, 78
Tang, X., & Chevalier, R. A. 2012, ApJ, 752, 83
Torii, K., Slane, P. O., Kinugasa, K., Hashimotodani, K., & Tsunemi, H. 2000, PASJ, 52, 875
Torres, D. F., Cillis, A., Martín, J., & de Oña Wilhelmi, E. 2014, JHEAp, 1, 31
Torres, D. F., Cillis, A. N., & Martín Rodriguez, J. 2013, ApJL, 763, L4
Velusamy, T., & Becker, R. H. 1988, AJ, 95, 1162
Vorster, M. J., & Moraal, H. 2013, ApJ, 765, 30
Wilson, A. S., & Weiler, K. W. 1976, A&A, 49, 357
Zank, G. P., & Matthaeus, W. H. 1992, JGR, 97, 17189
Zhang, L., Chen, S. B., & Fang, J. 2008, ApJ, 676, 1210
Zhou, Y., & Matthaeus, W. H. 1990, JGR, 95, 14881
Zhu, B.-T., Lu, F.-W., & Zhang, L. 2023, ApJ, 943, 89
Zhu, B.-T., Lu, F.-W., Zhou, B., & Zhang, L. 2021, A&A, 655, A41
Zrake, J., & Arons, J. 2017, ApJ, 847, 57